

Quantification of nonlinear seismic response of rectangular liquid tank

Santosh Kumar Nayak^a and Kishore Chandra Biswal*

Department of Civil Engineering, National Institute of Technology Rourkela, Odisha, India

(Received September 3, 2012, Revised July 18, 2013, Accepted August 7, 2013)

Abstract. Seismic response of two dimensional liquid tanks is numerically simulated using fully nonlinear velocity potential theory. Galerkin-weighted-residual based finite element method is used for solving the governing Laplace equation with fully nonlinear free surface boundary conditions and also for velocity recovery. Based on mixed Eulerian-Lagrangian (MEL) method, fourth order explicit Runge-Kutta scheme is used for time integration of free surface boundary conditions. A cubic-spline fitted regriding technique is used at every time step to eliminate possible numerical instabilities on account of Lagrangian node induced mesh distortion. An artificial surface damping term is used which mimics the viscosity induced damping and brings in numerical stability. Four earthquake motions have been suitably selected to study the effect of frequency content on the dynamic response of tank-liquid system. The nonlinear seismic response vis-a-vis linear response of rectangular liquid tank has been studied. The impulsive and convective components of hydrodynamic forces, e.g., base shear, overturning base moment and pressure distribution on tank-wall are quantified. It is observed that the convective response of tank-liquid system is very much sensitive to the frequency content of the ground motion. Such sensitivity is more pronounced in shallow tanks.

Keywords: seismic response; frequency content; artificial damping; quantification; mixed Eulerian-Lagrangian

1. Introduction

Sloshing is basically a nonlinear physical phenomenon, characterized by unrestrained free surface motion of liquid in a moving container. Understanding sloshing phenomenon is of paramount importance to the design of partially filled liquid tank subjected to seismic motion or any other motion for that matter. Liquid storage tanks are important components of many life line structures, industrial facilities and many other human infrastructures across the board. More often than not such tanks remain partially filled. Threat to the structural safety and stability of these tanks due to liquid sloshing is of great concern in a broad class of practical problems exemplified as ground-supported and elevated liquid storage tanks, fuel tanks of launching vehicles, dynamics of liquid transporting vehicles and its control, sloshing in nuclear fuel storage pool, water waves in reservoirs, cargo tanks of LNG carriers with liquid storage tank as system component. Of them the

*Corresponding author, Ph.D., E-mail: kcb@nitrrkl.ac.in

^aPh.D. Student, E-mail: sknayak1970@gmail.com

seismic response of ground supported liquid tanks deserves a special attention and is the focus of the present investigation. The prediction of sloshing behaviour is imperative for structural safety and integrity of liquid-tank system. In extreme situations when either the amplitude of external excitation is very high or the excitation frequency is very close to the fundamental frequency of free sloshing liquid or the supporting structure, the motion of liquid in the container becomes violent and creates highly localized impact pressures on the tank wall which may cause structural damage. The failure of such structures is not just critical to the huge economic value of the tank but has far reaching ramifications in terms of environmental hazards and human health. In fact heavy damages have been reported due to strong earthquakes such as Nigaata in 1964, Alaska in 1964, Parkfield in 1966, Imperial County in 1979, Coalinga in 1979, Loma Prieta in 1989, Landers in 1992, Northridge in 1994, Kocaeli earthquake in 1999, and very recently 2010 Maule, 2010-11 Christchurch and 2011 Tohoku-Pacific earthquake. The seismic design standards have been revised several times to improve the performance of tanks during future earthquakes. The dynamic response of fluid-structure system is very sensitive to the characteristics of ground motion and configuration of the system (Housner 1963, Haroun 1984, Haroun and Ellaithy 1984, Haroun 1983, Haroun and Tayel 1985).

Seismic mishap is the most likely and uncalled for threat to the structural safety and integrity of the liquid tank. Unlike other natural disasters, earthquakes are neither predictable nor preventable and their characteristics are highly nonlinear and complex. Hence the only resort open for the engineering community is to accurately predict the dynamic behaviour and properly design the fluid-structure system to minimize the effect of earthquake so that the tank-liquid system can stand the test of nature. Although the complicated deformed configurations of liquid storage tanks and the interaction between the fluid and the structure result in a wide variety of possible failure mechanisms, reports from past earthquakes indicate that the damages to the liquid filled tanks are either by large axial compression due to beamlike bending of the container wall causing a failure characterized as “elephant-foot” buckling or by sloshing of the contained liquid with insufficient freeboard. Markedly different failure types have been reported in cases of anchored and unanchored tanks (Leon and Kausel 1986, Lau *et al.* 1996, Malhotra 1996, Bakhshi and Hassanikhah 2008). The seismic response of elevated broad and slender liquid storage tanks isolated by elastomeric or sliding bearing was studied by Seleemah and El-Sharkawy (2011).

Most of the earlier researchers have studied the effect of nonlinearity on the sloshing response with regard to harmonic excitation and many of them have studied the effect only in term of variation in free surface sloshing elevation which although a crucial sloshing behaviour and the accuracy of its calculation is a key of estimation of hydrodynamic forces, yet not the complete information in the sense of dynamic response of the tank-liquid system in so far as the safety of the tank is concerned (Faltinsen 1978, Wu and Taylor 1994, Romero and Ingber 1995, Pal *et al.* 2003, Biswal *et al.* 2006, Virella *et al.* 2008, Pal and Bhattacharyya 2010, Cho and Lee 2004, Chen and Chiang 1999). The excitation due to seismic motion cannot be characterized by harmonic input. Ground shaking resulting from a seismic event is stochastic in nature, and this excitation may contain a wide array of frequencies. Very few works on seismic response of liquid tank is available. Choun and Yun (1999) used a linear analytical model to study the seismic behaviour of rectangular liquid tank with submerged block. Mitra *et al.* (2007) in their pressure based linear Finite Element model studied the dynamic response of rectangular tank with submerged internal components. They considered the ground motion of El Centro EW only for the investigation. Chen *et al.* (1996) used finite difference method to study the nonlinear response of rectangular tank using seismic ground motion records. Hernandez-Barrios *et al.* (2007) in their finite difference

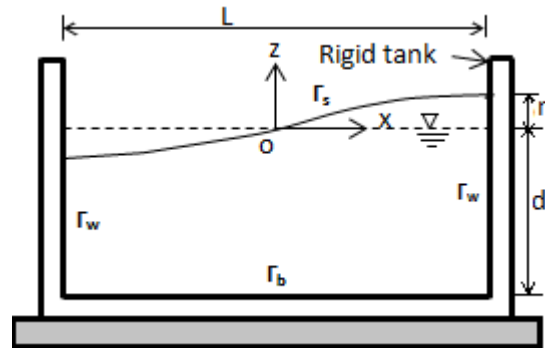


Fig. 1 Schematic diagram of rigid tank-liquid system

schemes studied nonlinear seismic response of cylindrical liquid tanks using semi-implicit and Cranck-Nicholson schemes. Chen *et al.* (2007) in their BEM based three dimensional sloshing analysis investigated the sloshing behaviour of rectangular and cylindrical tanks subjected to harmonic and seismic excitations. All the above researchers have concentrated their study simply on the logic of overall peak hydrodynamic response. The evaluation of absolute maximum hydrodynamic response as design parameter is not complete. Not much effort has been put to quantify the dynamic response of liquid tank in terms of impulsive and convective response components (Chen *et al.* 1996, Hernandez-Barrios *et al.* 2007, Chen *et al.* 2007). Hitherto, quantification of nonlinear seismic response in terms of impulsive and convective response components vis a vis frequency content of ground motion is not reported in the literature.

2. Mathematical modelling of tank-liquid system

Fig. 1 shows the problem geometry for the tank-liquid system. The Cartesian coordinate system O-xz for the computational domain of the liquid is defined such that the origin is at the center of the still free surface with z-axis pointing vertically upward. The liquid is assumed to be inviscid and incompressible and the flow is irrotational. For such an ideal liquid, the velocity distribution can be derived from a scalar function called *velocity potential* $\phi(x, y, t)$ which describes the motion of liquid through satisfaction of Laplace (continuity) equation

$$\nabla^2 \phi = 0 \quad (1)$$

which governs the potential flow in the fluid domain Ω . Eq. (1) is elliptic in nature and requires both free surface and body surface boundary conditions for simulation of nonlinear sloshing wave problem. The boundary conditions are described as follows.

2.1 Nonlinear free surface boundary conditions

On the time dependent free surface boundary Γ_s , both kinematic and dynamic boundary conditions need to be satisfied at any instant and on the exact free surface. The kinematic boundary condition requires that the fluid particle once on the free surface remains always on the free surface. Based on Eulerian description the free surface kinematic boundary condition is given by

$$\frac{\partial \eta}{\partial t} = \frac{\partial \phi}{\partial z} - \frac{\partial \phi}{\partial x} \frac{\partial \eta}{\partial x} \quad \text{on } \Gamma_s \quad (2)$$

where $\eta(x, z, t)$ is the instantaneous free surface wave elevation.

The dynamic boundary condition requires that the pressure on the free surface be uniform and equal to the external atmospheric pressure. This boundary condition can be obtained from Bernoulli equation with the assumption of zero atmospheric pressure. An artificial damping term may be suitably introduced into the boundary condition which not only accounts for the effect of viscosity in dissipating the momentum by opposing the fluid motion but also brings in numerical stability. The damping modified unsteady Bernoulli's equation may be expressed as

$$\frac{\partial \phi}{\partial t} = -g\eta - \frac{1}{2} \nabla \phi \cdot \nabla \phi - \mu \phi \quad \text{on } \Gamma_s \quad (3)$$

where g is the gravitational acceleration and μ is the artificial damping term.

2.2 Body surface boundary condition

On the walls of the tank the velocity of liquid is equal to the wall velocity in normal direction

$$\frac{\partial \phi}{\partial n} = V_n \quad \text{on } \Gamma_w \quad (4)$$

where V_n is the instantaneous velocity of the vertical wall subjected to horizontal ground acceleration and n is the normal to the wall surface pointing out of the liquid domain.

On the rigid bottom supported on rigid foundation, no flux condition needs to be satisfied.

$$\frac{\partial \phi}{\partial n} = 0 \quad \text{on } \Gamma_b \quad (5)$$

Thus Eqs. (1) - (5) defines the initial and boundary value problem with nonlinear free surface boundary conditions. The nonlinearity in free surface boundary condition is attributed to: (1) *a priori* unknown free surface elevation at any given instant and (2) kinematic and dynamic boundary conditions in Eqs. (2) and (3) as they contain second order differential terms.

The set of Eqs. (1)-(5) are elliptic in space and parabolic in time. Mixed-Eulerian-Lagrangian method due to Longuet-Higgins and Cokelet (1976) is used for numerical solution of the system of equations. In mixed-Lagrangian-Eulerian the surface nodes called 'markers' are allowed to move with the same velocity as the liquid. In this procedure the spatial equations are solved in Eulerian (fixed grid) frame and the integration of the free surface boundary conditions is executed in Lagrangian manner. This requires the free surface boundary conditions in Eqs. (2) and (3) to be written in Lagrangian form as follows.

$$\frac{d\phi}{dt} = -g\eta + \frac{1}{2} \nabla \phi \cdot \nabla \phi - \mu \phi \quad \text{on } \Gamma_w \quad (6)$$

$$\frac{dx}{dt} = \frac{\partial \phi}{\partial x}; \quad \frac{dz}{dt} = \frac{\partial \phi}{\partial z} \quad (7)$$

After obtaining the time derivative of velocity potential, the nonlinear hydrodynamic pressure can be calculated by using the following equation

$$p = -\rho \left(\frac{\partial \phi}{\partial t} + \frac{1}{2} |\nabla \phi|^2 + \mu \phi \right) \quad (8)$$

The base shear S_b and overturning base moment M_b can be calculated by the following expression

$$S_b = \int_{\Gamma_w} p \, d\Gamma_w \quad (9)$$

$$M_b = \int_{\Gamma_w} (p \, dz)z + \int_{\Gamma_b} (p \, dx)x \quad (10)$$

Impulsive pressure may be determined by assuming the whole liquid as a rigid solid block without convective mass. This assumption ignores the sloshing of the liquid and hence the convective response. As a consequence of this, the pressure at the quiescent liquid free surface vanishes at every instant during the motion.

$$\frac{\partial \phi}{\partial t}(x, 0, t) = 0 \quad (11)$$

3. Finite element formulation

The entire liquid domain Ω , bounded by body surface Γ_w , tank bottom Γ_b and free surface Γ_w , is discretized by four-noded quadrilateral elements for finite element formulation and solution of Laplace equation for Dirichlet boundary condition (ϕ) on the free surface and Neumann boundary condition ($\nabla \phi$) on the body surface. The velocity potential may be approximated as

$$\phi \approx \bar{\phi}(x, z, t) = \sum_{j=1}^n \phi_j N_j(x, z) \quad (12)$$

where ϕ_j are time dependent nodal velocity potentials, N_j are shape functions and n is the number of nodes. Application of Galerkin's weighted-residual method to Laplace equation gives rise to

$$\int_{\Omega} \nabla^2 \phi N_i \, d\Omega = 0 \quad (13)$$

Since

$$\nabla(\nabla \phi N_i) = \nabla^2 \phi N_i + \nabla \phi \nabla N_i \quad (14)$$

Eq. (14) may be written as

$$\int_{\Omega} [\nabla(\nabla \phi N_i) - \nabla \phi \nabla N_i] \, d\Omega = 0 \quad (15)$$

Application of Gauss theorem produces

$$\int_{\Gamma} N_i \frac{\partial \phi}{\partial n} \, d\Gamma - \int_{\Omega} \nabla \phi \nabla N_i \, d\Omega \quad (16)$$

where $\Gamma = \Gamma_w \cup \Gamma_b \cup \Gamma_s$, is the boundary of the liquid domain Ω . Substitution of the approximation function for the potential and the boundary conditions into the above equation yields

$$\int_{\Omega} \nabla N_i \sum_{j=1}^n \phi_j \nabla N_j \, d\Omega \Big|_{j \in \Gamma_s} = \int_{\Gamma_w} N_i V_n - \int_{\Omega} \nabla N_i \sum_{j=1}^n \phi_j \nabla N_j \, d\Omega \Big|_{j \in \Gamma_s} \quad (17)$$

where Γ_s and Γ_b are the free surface and body (vertical wall) surface respectively on which the potential and its normal derivatives are prescribed. The potential on the free surface is known from the free surface boundary condition and the terms corresponding to the surface nodes have therefore been taken to the right hand side. This scheme suggested by Wu and Eatock Taylor (1994) was found to be effective in dealing with the singularity at the intersection point between the body surface and free surface on account of the confluence of boundary conditions.

Eq. (17) may be expressed in matrix form as

$$[K]\{\phi\} = [F] \quad (18)$$

where

$$K_{ij} = \int \nabla N_i \nabla N_j \, d\Omega \quad (19)$$

$$F_i = \int_{\Gamma_w} N_i V_n - \int_{\Omega} \nabla N_i \sum_{j=1}^n \phi_j \nabla N_j \, d\Omega \Big|_{j \in \Gamma_s} \quad (20)$$

where K_{ij} is the global fluid matrix and F_i is the global right hand side vector. It must be mentioned that the matrix K_{ij} in Eq. (19) varies with time for fully nonlinear problem.

Numerical evaluation of the dynamic and kinematic boundary conditions, Eqs. (6)-(7), requires an approximation of velocity at the free surface. Although, direct differentiation of potential approximation via shape functions is a convenient option to obtain the velocity, shape functions however do not guarantee the continuity of its derivatives at the boundary of the elements and may result in lower order, discontinuous velocity with compromised accuracy. The velocity continuity can be ensured by use of higher order FE for potential approximation. In the present study, however C^0 isoparametric rectangular element is used. In order to avoid excessive accumulation of error in the time stepping procedure, the following method is used for velocity recovery.

The two dimensional velocity vector, $U = u \hat{i} + v \hat{j}$ may be approximated in terms of the same shape functions as used for velocity potential.

$$U = \sum_{j=1}^n u_j N_j(x, z) \quad (21)$$

Galerkin weighted-residual method is used to approximate the relationship $\nabla \phi = U$, in the form

$$\int_{\Omega} N_i (\nabla \phi - U) \, d\Omega = 0 \quad (22)$$

Substitution of Eqs. (12) and (21) into Eq. (22) yields

$$\int_{\Omega} N_i \frac{\partial N_j}{\partial n} \phi_j \, d\Omega = \int_{\Omega} N_i N_j U_j \, d\Omega \quad (23)$$

In matrix form the above equation can be expressed as

$$[C]\{u\} = [D_1]\{\phi\} \quad (24)$$

$$[C]\{v\} = [D_2]\{\phi\} \quad (25)$$

where

$$[C] = \int_{\Omega} N_i N_j \, d\Omega \quad (26)$$

$$[D_1] = \int_{\Omega} N_i \frac{\partial N_j}{\partial x} N_j \, d\Omega \quad (27)$$

$$[D_2] = \int_{\Omega} N_i \frac{\partial N_j}{\partial z} N_j \, d\Omega \quad (28)$$

and u_i and v_i are the components of velocity vector U_j at node j .

From the velocities thus obtained, the updated position of the free surface at the start of the next time step can be found using Eq. (7). The updated value of the velocity potential on the free surface can also be determined from Eq. (6). A new finite element mesh is then generated corresponding to the updated geometry which requires further solution of Laplace equation in the spatial domain, recovery of velocity and time-integration of kinematic and dynamic boundary conditions to advance the solution in time domain.

4. Implementation of numerical scheme

As stated above the implementation and accuracy of the numerical scheme developed involves five steps: (1) mesh generation or discretization of liquid domain, (2) the solution of FE-discretized Laplace equation in spatial domain, (3) recovery of velocity by global projection method, (4) surface tracking and location of the new position of Lagrangian free surface nodes by effective time-integration scheme, and (5) regriding at each time step or after a certain number of time steps in order to avoid inordinate concentration of Lagrangian free surface nodes in the region of higher gradients and have control over the minimum grid size for a given time step. Of the five steps mentioned above steps (2) and (3) have been discussed in earlier paragraphs and the rest of the steps are discussed in the following paragraph.

4.1 Mesh generation

The liquid domain is discretized by four noded isoparametric quadrilateral elements. The entire liquid domain in the tank is divided in the x-direction by $nx+1$ uniformly placed vertical lines at as many surface nodes. The liquid depth is divided into mz number of meshes with $mz+1$ numbers of nodes in the vertical direction. Reduced mesh height is provided near the free surface in order that

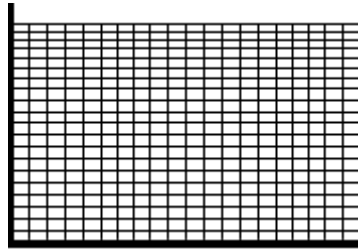


Fig. 2 Typical finite element mesh

pronounced sloshing near the free surface can be better captured. The locations of free surface nodes change with time due to the Lagrangian characteristics. The total number of nodes and elements are computed as $(nx+1) \times (nz+1)$ and $(nx) \times (nz)$, respectively. A representative finite element mesh discretizing the liquid domain is shown in Fig. 2.

4.2 Time integration

In material node approach ($\nabla\phi = \vec{v}$) of MEL method the surface nodes move with the fluid particles at the corresponding nodes and thus mesh distortion takes place. Fourth order explicit Runge-Kutta time-integration scheme is used to trace the moving nodes on the free surface and determine the associated velocity potential and other unknown variables of interest. The coordinates (x,z) and velocity potential at time t may be represented by a single variable as $Q_t(x, z, \phi)$ and expressed in matrix form as follows.

$$Q_t = (x_t, z_t, \phi_t)^T$$

$$x_t = (x_1, x_2, x_3, \dots, x_{nx+1})^T$$

$$z_t = (z_1, z_2, z_3, \dots, z_{nx+1})^T$$

$$\phi_t = (\phi_1, \phi_2, \phi_3, \dots, \phi_{nx+1})^T$$

Where $(x_i, z_j)_{i,j=1, 2, \dots, nx+1}$ and $(\phi_i)_{i=1, 2, \dots, nx+1}$ respectively represent the coordinates and velocity potentials of the nodes, along the free surface and nx is the number of liquid elements in the x -direction. The total derivative of Q_t with respect to time is written as

$$\frac{DQ_t}{Dt} = \left(\begin{matrix} \frac{Dx_t}{Dt} & \frac{Dz_t}{Dt} & \frac{D\phi_t}{Dt} \end{matrix} \right) = F(t, Q_t)$$

The coordinates and velocity potential of the free surface nodes at the subsequent time step $t + \Delta t$ are obtained from the following relation.

$$Q_{t+\Delta t} = Q_t + \frac{Q_1}{6} + \frac{Q_2}{3} + \frac{Q_3}{3} + \frac{Q_4}{6}$$

Where

$$Q_1 = \Delta t F(t, Q_t)$$

$$Q_2 = \Delta t F(t + \Delta t, Q_t + Q_1 / 2)$$

$$Q_3 = \Delta t F(t + \Delta t / 2, Q_t + Q_2 / 2)$$

$$Q_4 = \Delta t F(t + \Delta t, Q_t + Q_3)$$

4.3 Regridding

At the beginning of the numerical simulation, the free surface nodes are uniformly distributed in the x-direction on the quiescent free surface with a zero surface elevation. As time elapses, the Lagrangian nodes on the liquid free surface move and such movement leads to unequal horizontal spacing and gradual concentration of Lagrangian particles in the region of steep gradient close to the tank wall. The mesh distortion thus occurs may lead to numerical instability. To eliminate such instabilities, a mesh regridding technique is used at every time step. The numerical experiments conducted by Dommermuth and Yue (1987) showed that the regridding is extremely effective and eliminates the numerical instabilities without the use of artificial smoothing. A cubic spline is fitted through the distorted Lagrangian nodes on the free surface. Subsequently, the velocity potentials and associated boundary values on the new sets of uniformly spaced Lagrangian nodes are obtained by interpolation. The liquid domain is remeshed based on the positions of newly formed Lagrangian nodes.

5. Model validation

The numerical scheme, based on FEM, developed as above is coded and executed in Matlab platform for model validation and evaluation of the seismic response of partially filled rectangular liquid-tank system.

5.1 Problem definition and linear model validation

The governing parameters of the two-dimensional tank-liquid system are as follows: $L = 10$ m, $d = 5$ m, density of liquid, $\rho = 1000\text{kg/m}^3$, artificial damping (pseudo-viscous damping), $\mu = \zeta\mu_{crit}$ where ζ is the viscous type numerical damping; $\mu_{crit} = 2\omega$ and ω is the fundamental sloshing frequency of liquid.

The correct prescription of the value of ζ depends on the dimension of the tank and liquid depth and can be found from experimental validation of numerical result. In the present investigation, however, the value of ζ has been determined by comparing the present linear numerical result with the analytical result due to Choun and Yun (1999). El Centro-EW is prescribed as ground motion for computation of time history of sloshing. The result obtained with a prescribed artificial viscous damping $\zeta = 0.0075$ is plotted in Fig. 3 along with the analytical result and is found to have extremely close matching in all its characteristics such as magnitude and phase etc. The value of ζ so obtained is used for subsequent computations and observed to have given numerically stable result for all the ground motions.

5.2 Non-linear model validation

In order to validate the nonlinear FEM model developed for the present study, numerical simulation of sloshing was conducted in a tank of width $L = 30.675$ m and liquid depth $d = 10.73$ m. A harmonic force of $a_t = 0.01g \sin \bar{\omega}t$ is applied as base excitation, where $\bar{\omega}$ is taken as the fundamental sloshing frequency ω_1 of the liquid. The comparative result of temporal variation of free surface sloshing elevation measured at right end of the tank is presented in Fig. 4. It can be

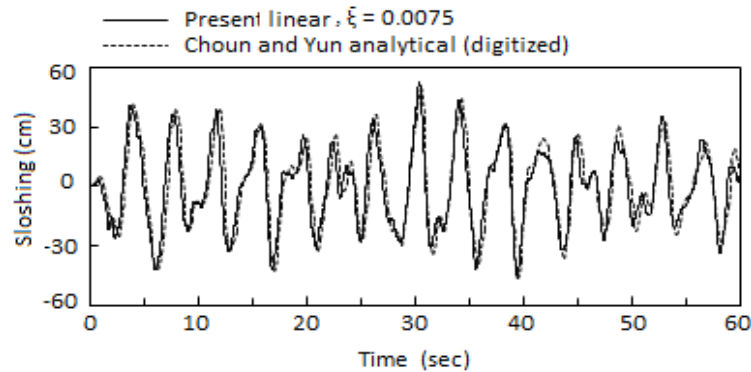


Fig. 3 Time history of free surface sloshing amplitude at left hand wall of tank due to horizontal ground motion of El Centro-EW

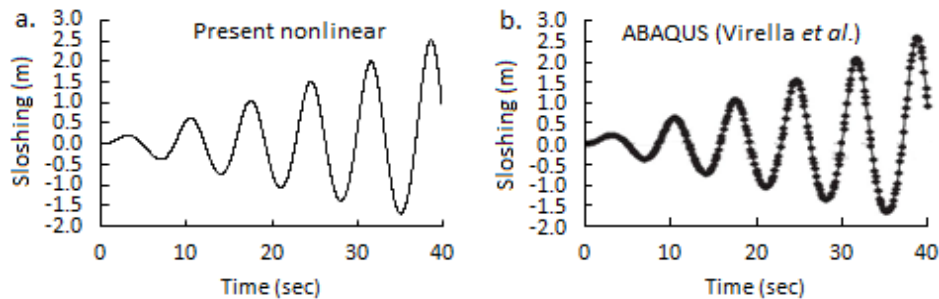


Fig. 4 Time history of the nonlinear sloshing elevation at right hand wall of tank in the first sloshing mode for the model with $d/L = 0.35$

clearly observed that the result of the proposed model is in an excellent agreement with the result obtained by Virella *et al.* (2008) using commercial software ABAQUS.

6. Seismic response and discussion

Numerical experiment is conducted taking the same tank dimensions and governing parameters as in Choun and Yun (1999) for the nonlinear seismic response of tank-liquid system. Four different ground motion data presented in Table 1 are used as the excitations for the system. The PGAs of all the records are scaled to a fixed magnitude of 0.2g as shown in Fig. 5 for comparison of the dynamic responses under seismic excitations with varying frequency contents. On the basis of the ratios of PGA/PGV, El Centro-EW, Imperial Valley, Landers and San-Francisco earthquakes are considered as low, low, intermediate and high frequency content seismic motions, respectively. In addition, the power spectrum density functions (PSDF) of all ground motions are obtained which depict the frequency content as shown in Fig. 6.

6.1 Hydrodynamic responses

The hydrodynamic responses in terms of sloshing elevation, base shear, overturning base moment, pressure distribution on the tank wall are computed for ground motions of different

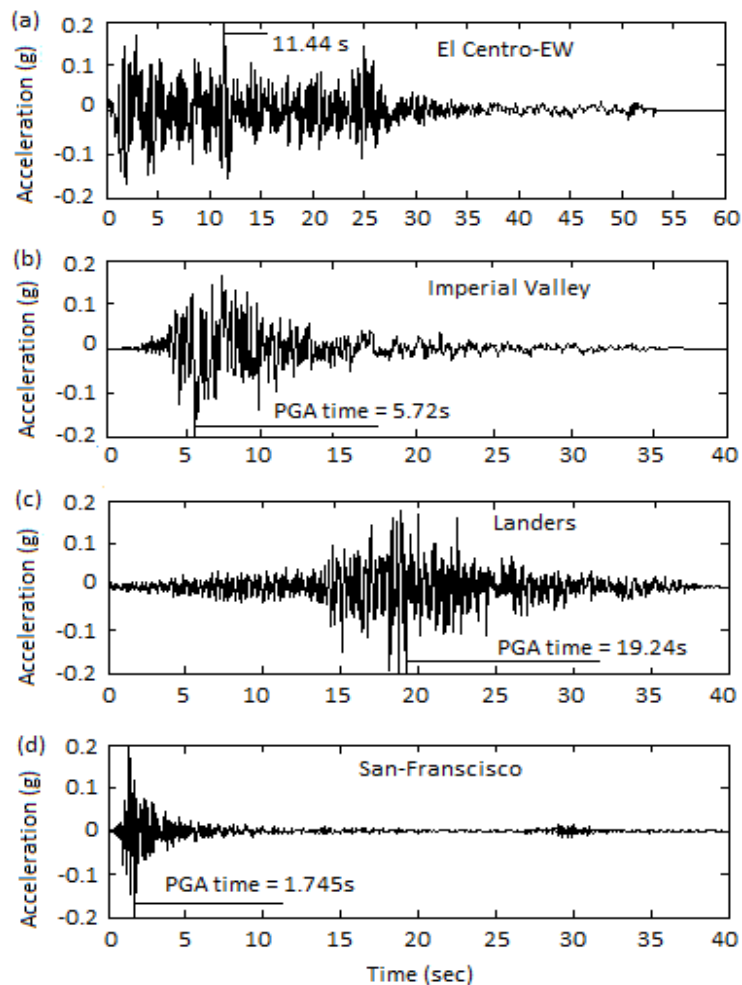


Fig. 5 Time-history of acceleration of ground motions: (a) El Centro EW (b) 1979 Imperial 185 (c) 1992 Landers 855 (d) 1957 San-Francisco 23

frequency content. The effect of nonlinearity of sloshing wave on each of these quantities is probed. The impulsive and convective response components are computed and their contribution to the overall hydrodynamic forces are studied and quantified.

6.1.1 Sloshing response

The sloshing wave elevation is not only important for the seismic-safety design of liquid containers but also gives the convective response of hydrodynamic pressure and associated base shear and base moment. Free board to be provided in a tank is based on maximum value of sloshing wave height. Further, insufficient free board obstructs the free movement of convective mass and thus changes the amount of liquid in convective mode. If sufficient free board is not provided roof structure should be designed to resist the uplift pressure due to sloshing of liquid. Hence sensitiveness of sloshing response to the frequency content of seismic ground motions is studied.

Table 1 Ground motion records

Records (Station)	Component	Magnitude	Epicentral Distance (Km)	Duration (s)	Time step for response computation (s)	PGA (g)	PGV (m/s)	PGA/PGV
1940 El Centro-EW ^a	-	-	-	60	0.02	0.2141	0.4879	0.439
1979 Imperial Valley-06 (Holtville Post office)	HVP225	6.53	19.81	37.745	0.005	0.2476	0.4765	0.519
1992 Landers (Fort Irwin)	FTI000	7.28	120.99	40.0	0.02	0.1288	0.1244	1.035
1987 San-Francisco (Golden Gate Park)	GGP010	5.28	11.13	39.725	0.005	0.1073	0.0377	2.846

^a All other ground motion records except the superscripted earthquake are taken from Pacific Earthquake Engineering Research Next Generation Attenuation (PEER-NGA) strong motion database records available online at <http://peer.berkeley.edu/nga>.

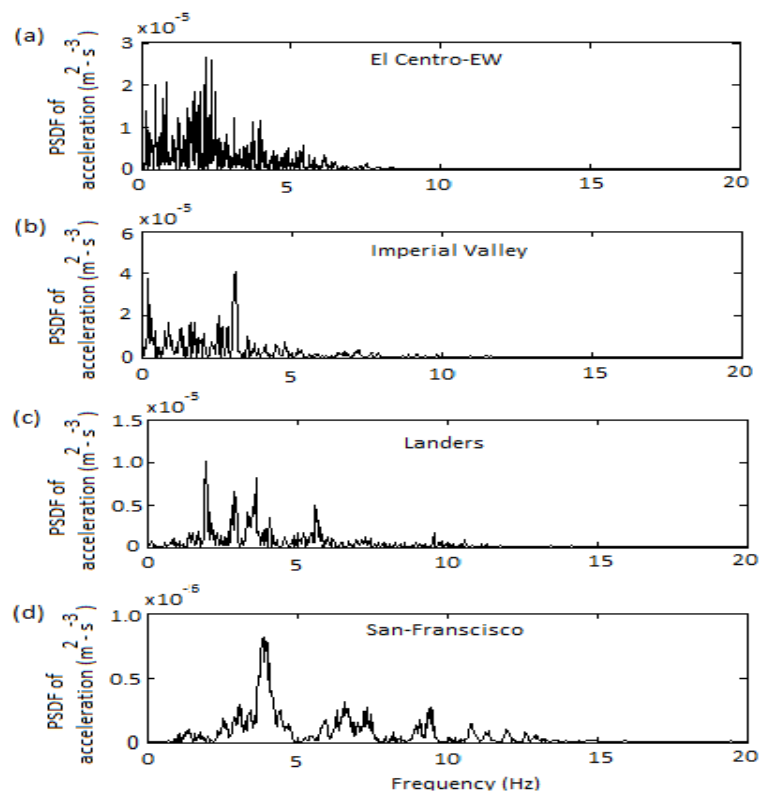


Fig. 6 Power spectral density function (PSDF) of ground acceleration: (a) El Centro-EW (b) Imperial Valley (c) Landers (d) San-Francisco

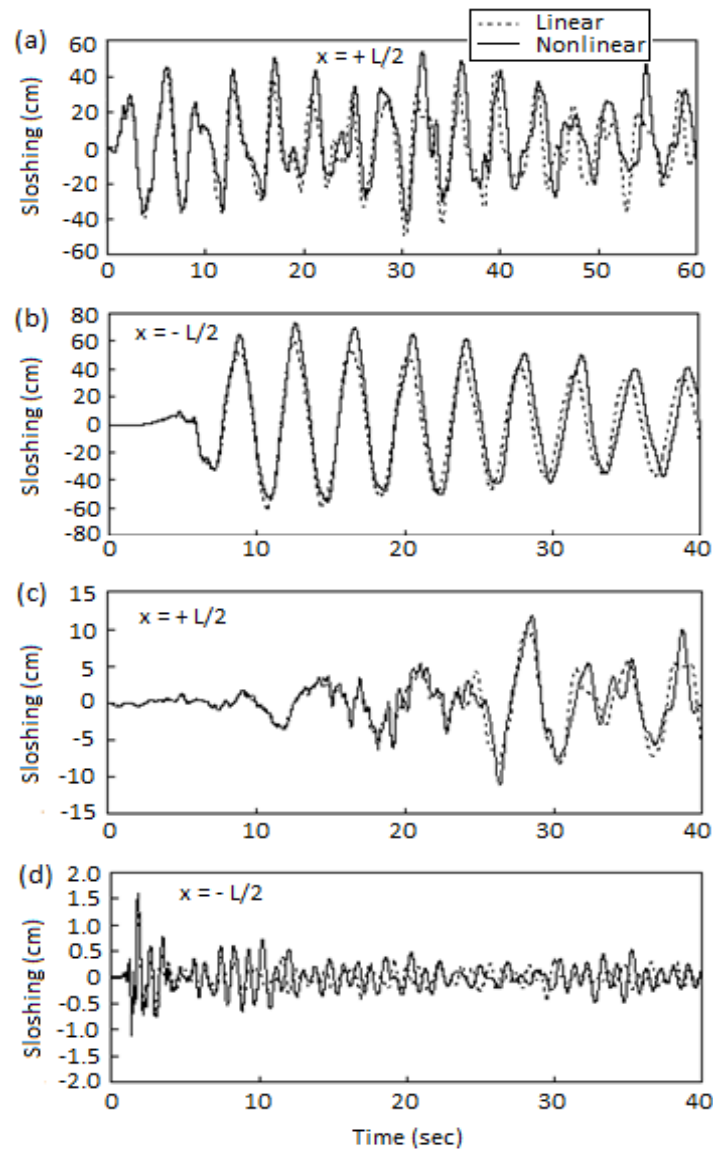


Fig. 7 Temporal variation of linear and nonlinear sloshing elevation due to ground motions: (a) El Centro-EW (b) Imperial Valley (c) Landers (d) San-Francisco

The time history of surface wave elevations due to all the ground motions is presented in Fig. 7. It is observed that both for linear and nonlinear model, the sloshing elevation is significantly more due to low frequency ground motion of Imperial Valley. Linear and nonlinear positive sloshing amplitudes at $x = -L/2$ and $x = +L/2$ and the percentage increase in nonlinear response with respect to linear response are listed in Table 2. Maximum positive sloshing amplitude reduces from low to high frequency ground motions. The effect of nonlinearity on free surface sloshing elevation is more pronounced in case of low frequency ground motion of Imperial Valley. The increase in sloshing elevation has a decreasing trend from low to high frequency content seismic motion.

Table 2 Linear and nonlinear peak sloshing amplitude

Earthquake Record	Sloshing elevation (+ ve) $x = -L/2$			Sloshing elevation (+ ve) $x = +L/2$		
	Linear	Nonlinear	%	Linear	Nonlinear	%
	(cm)	(cm)	variation	(cm)	(cm)	variation
El-Centro EW	50.02	51.42	2.80	42.86	53.68	25.24
Imperial Valley	59.78	72.90	21.95	60.20	69.16	14.88
Landers	8.34	11.72	40.52	9.44	11.77	24.68
San-Francisco	1.21	1.60	32.23	0.93	1.13	21.50

6.1.2 Base shear and overturning base moment

The temporal history of base shear and overturning base moment due to horizontal ground motions of selected earthquakes are computed by the proposed method. The effect of frequency content on the hydrodynamic response of the tank-liquid system is probed. Both base shear and overturning base moment are quantified in terms of impulsive and convective components. It may be mentioned convective component is frequency sensitive while impulsive response is acceleration sensitive. The computed responses of base shear and base moment are presented in terms of their time history in Figs. 8 and 9 respectively.

The absolute maximum peaks of base shear and base moments due to all earthquakes are presented in Table 3. The responses are normalized with respect to those of the low frequency Imperial Valley record and presented in brackets. The table presents both linear and nonlinear responses of each physical parameter. As nonlinearity has nothing to do with the impulsive responses, their values remain the same under linear and nonlinear columns. The results show that impulsive responses remain almost unchanged irrespective of the frequency content of ground motions. However marginally higher values are observed in case of El Centro record. Unlike impulsive response, a wide variation in maximum values is recorded for convective components. The convective responses are magnified in case of El Centro earthquake. It is observed that there exists time lag between the peaks of impulsive and convective response components. For all earthquake records considered for the study, one can notice that the magnitudes of peak impulsive response is higher than the corresponding convective response irrespective of the frequency content of ground motions. The absolute peaks of impulsive responses invariably occur at the instant of PGAs of ground motions. The total seismic response is dominated by the impulsive response and occurs at some instant close to the time of PGA.

In some sense, the reader may find the results in Table 3 intriguing. To clarify the confusion and for completeness of quantification, the contribution of impulsive and convective response components to the absolute total structural response are presented in Table 4. From Table 3 it can be seen that both convective and impulsive response components of base shear are significantly more in case of El Centro-EW than their respective counterparts for Imperial Valley. However the absolute total base shear is more, although marginally, in case of low frequency Imperial Valley ground motion. An even more contrasting observation can be made in case of overturning base moment. It can be seen that the absolute maximum convective responses presented in Table 3 do not contribute to the absolute maximum total hydrodynamic responses. For a clearer picture, one can refer to the contributions of convective components to the absolute maximum total

hydrodynamic responses presented in Table 4. This is due to the time lag between the impulsive and convective peak responses. However the effect of absolute peak convective responses and/or local peaks cannot be marginalized or under estimated. This is because the amount of structural damage expected in an earthquake is proportional to the duration of the earthquake and this relationship is not linear. A longer duration of shaking causes the damage to increase. In case of long duration earthquakes amplified local peaks contribute to structural fatigue and may prove critical to the safety of the structure and hence their effect should be taken into account in design.

If sloshing of the liquid, hence the effect of convective response, is ignored as is done in some simplified analysis; all the response quantities are found more than those when sloshing is considered. This observation is made in case of Landers and San-Francisco records on the basis of linear analysis. This observation is shown with superscripted data in Table 4. This is due to the fact that convective responses for the said motions occur in opposite phase with respect to the impulsive responses and counter their effect.

The convective response in terms of sloshing elevation is important in such decisions as the correct estimation of free board between the quiescent free surface and tank cover and also in the design of roof cover which experiences convective hydrodynamic pressure in case of inadequate free board. Thus incorrect estimation of sloshing elevation may lead to under-designed free board which may result spillage of hazardous fluids or the failures in the tank roof.

It is evident from the tables that the effect of nonlinearity of surface wave on the dynamic response is more pronounced in case of low frequency earthquake of Imperial Valley and intermediate frequency content El Centro record. Figs. 10 and 11 present the comparative time history of convective responses of base shear and base moment due to Imperial Valley and El Centro records respectively. It is seen that nonlinear absolute global maximums in both the cases are significantly more than their linear counterparts. In addition, the nonlinear local peaks are consistently more, although not substantially, which may contribute to structural fatigue for long duration earthquakes and hence prove detrimental to the structural safety because of the cumulative damage sustained by the tank.

A shallow tank of $d/L = 0.2$ is considered to study the effect of nonlinearity of surface wave on the dynamic response of the tank-liquid system. The ground motion records of El Centro and Imperial Valley are used for the numerical experiment. Figs. 12 and 13 present the comparative result of time history of base shear and base moment for tall tank ($d/L = 0.5$) and shallow tank ($d/L = 0.2$) respectively due to the above said ground motions. In case of shallow tanks, early dominance of convective response is noticed when the impulsive response is still in the dominating stage, and both impulsive and convective responses are in the same phase. As a result, an increase in overall total hydrodynamic response can be observed in case of shallow tank. From a comparative study of Figs. 12(b) and 13(b) it can be seen that although the convective and impulsive response of base shear for shallow tanks follow the same trend both in terms of phase and magnitudes, the two significantly differ in magnitudes in their respective responses to overturning base moments. This fact is attributed to higher convective pressure resultant height due to amplified sloshing for low frequency motion of Imperial Valley. As these forces are applied high up the tank they tend to cause overturning rather than sliding. This is in consistent with the physics that long period motions cause high surface waves in the tanks which apply large convective forces to the side of the tank. The histograms in Figs. 14 and 15 show respectively the absolute peak responses and contributions of impulsive and convective components to absolute peak responses.

Table 3 Absolute maximum dynamic response of various physical parameters of the tank liquid system

Records	Dynamic responses	Hydrodynamic response					
		Linear			Nonlinear		
		Impulsive	Convective	Total	Impulsive	Convective	Total
El-Centro EW	Sloshing (cm)	-	50.02 (0.83)	50.02 (0.83)	-	53.68 (0.74)	53.68 (0.74)
	Base shear (kN/m)	54.87 (1.14)	12.27 (0.71)	60.83 (1.01)	54.87 (1.14)	47.50 (2.10)	59.20 (0.98)
	Base moment (kN.m/m)	216.69 (1.11)	70.14 (0.72)	248.34 (0.99)	216.69 (1.11)	216.95 (1.72)	228.30 (0.93)
Imperial Valley	Sloshing (cm)	-	60.20 (1.0) ^a	60.20 (1.0)	-	72.90 (1.0)	72.90 (1.0)
	Base shear (kN/m)	48.13 (1.0)	17.15 (1.0)	60.03 (1.0)	48.13(1.0)	22.68 (1.0)	60.50 (1.0)
	Base moment (kN.m/m)	195.40 (1.0)	97.12 (1.0)	250.19 (1.0)	195.40 (1.0)	126.11 (1.0)	245.45 (1.0)
Landers	Sloshing (cm)	-	9.44 (0.16)	9.44 (0.16)	-	11.77 (0.16)	11.77 (0.16)
	Base shear (kN/m)	48.16 (1.0)	3.15 (0.18)	46.92 (0.78)	48.16 (1.0)	29.39 (1.30)	42.71 (0.71)
	Base moment (kN.m/m)	196.64 (1.0)	19.30 (0.20)	189.70 (0.76)	196.64 (1.0)	120.45 (0.96)	170.95 (0.69)
San- Francisco	Sloshing (cm)	-	1.21 (0.02)	1.21 (0.02)	-	1.60 (0.02)	1.60 (0.02)
	Base shear (kN/m)	48.75 (1.01)	0.18 (0.01)	48.58 (0.81)	48.75 (1.01)	10.68 (0.47)	47.63 (0.79)
	Base moment (kN.m/m)	197.40 (1.01)	0.94 (0.01)	196.49 (0.79)	197.40 (1.01)	43.17 (0.34)	192.31 (0.78)

^aThe bracketed values are normalized hydrodynamic responses with respect to low frequency earthquake of Imperial Valley

Table 4 Contributions of impulsive and convective components for absolute maximum hydrodynamic response of various physical parameters

Records	Dynamic responses	Hydrodynamic response					
		Linear			Nonlinear		
		Impulsive	Convective	Total	Impulsive	Convective	Total
El-Centro EW	Base shear (kN/m)	54.87	5.96	60.83	52.24	6.96	59.20
	Base moment (kN.m/m)	216.69	31.65	248.34	206.07	22.23	228.30
Imperial Valley	Base shear (kN/m)	45.53	14.50	60.03	44.43	16.37	60.50
	Base moment (kN.m/m)	167.39	82.80	250.19	140.38	105.07	245.45
Landers	Base shear (kN/m)	47.52	0.60 [#]	46.92	41.33	1.37	42.71
	Base moment (kN.m/m)	192.83	3.13 [#]	189.70	168.80	2.15	170.95
San-Francisco	Base shear (kN/m)	48.75	0.17 [#]	48.58	45.82	1.81	47.63
	Base moment (kN.m/m)	197.40	0.91 [#]	196.49	185.54	6.77	192.31

[#]The superscripted values indicate that the convective responses are in opposite phase with their impulsive counterparts.

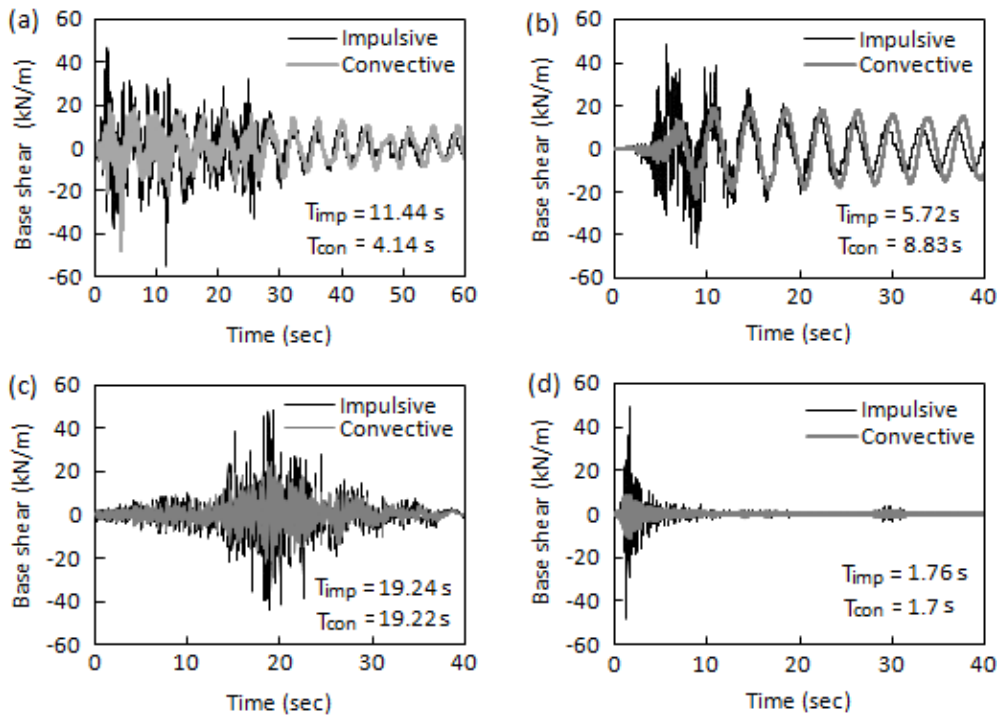


Fig. 8 Time history of impulsive and convective responses of base shear: (a) El Centro-EW (b) Imperial Valley (c) Landers (d) San-Francisco

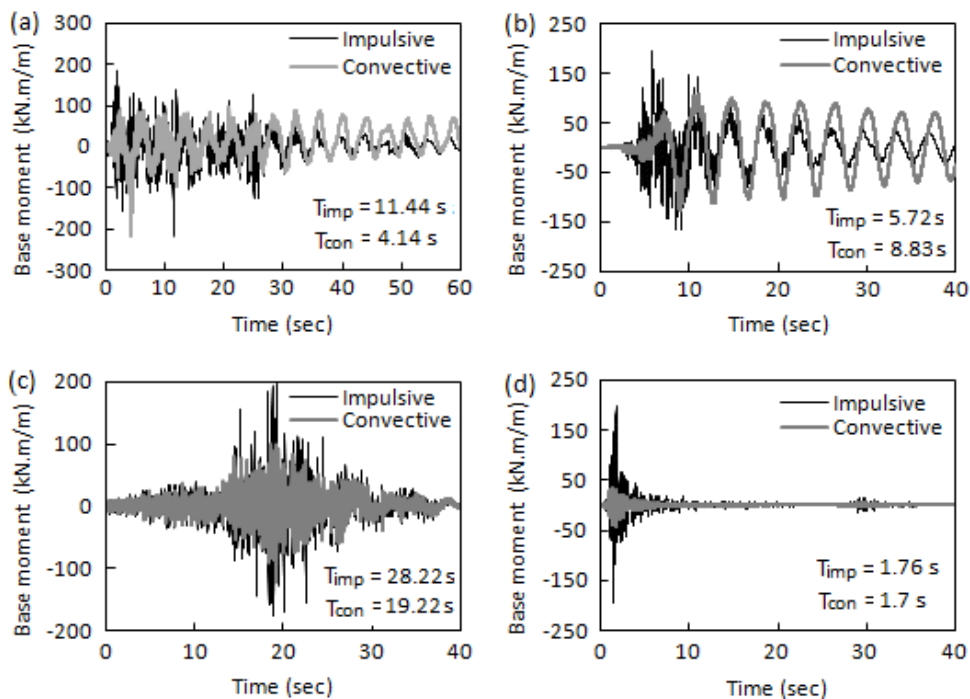


Fig. 9 Time history of impulsive and convective responses of base moment: (a) El Centro-EW (b) Imperial Valley (c) Landers (d) San-Francisco

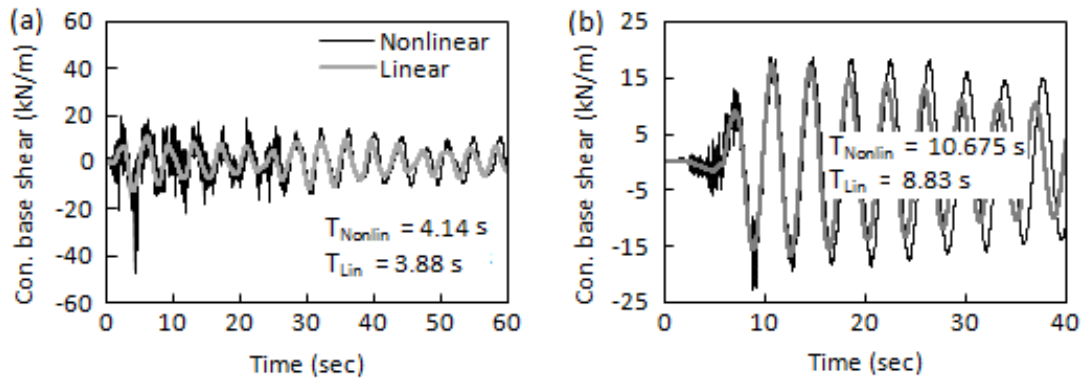


Fig. 10 Time history of linear and nonlinear convective base shear: (a) El Centro-EW (b) Imperial Valley

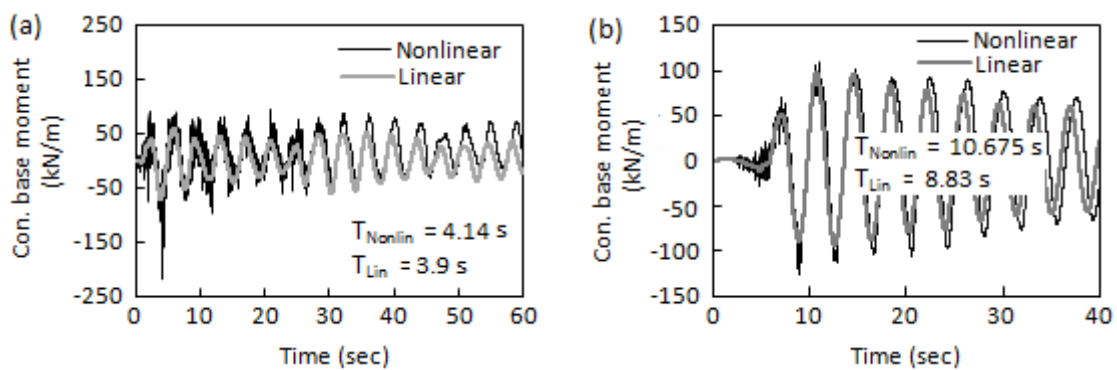


Fig. 11 Time history of linear and nonlinear convective base moment: (a) El Centro-EW (b) Imperial Valley

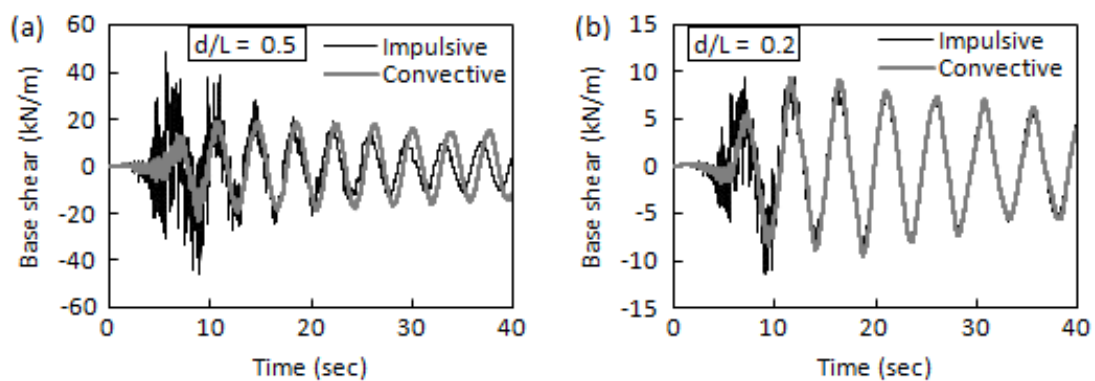


Fig. 12 Time history of impulsive and convective responses of base shear for Imperial Valley ground motion: (a) $d/L = 0.5$ (b) $d/L = 0.2$

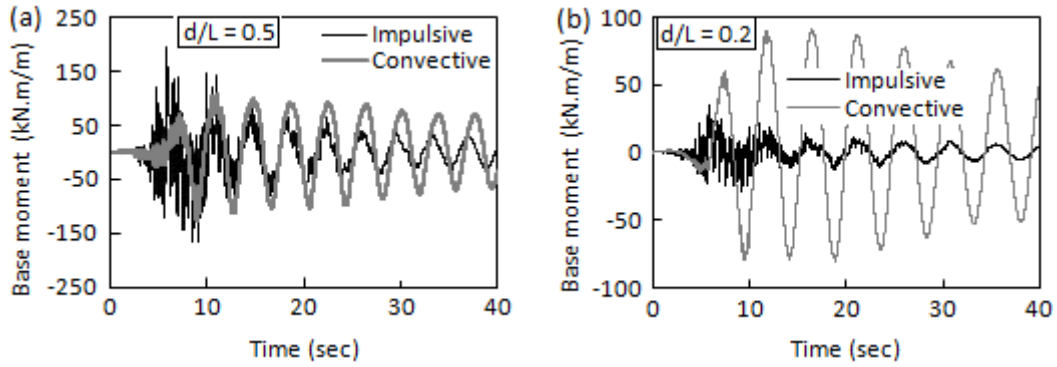


Fig. 13 Time history of impulsive and convective responses of base moment for Imperial Valley ground motion: (a) $d/L = 0.5$ (b) $d/L = 0.2$

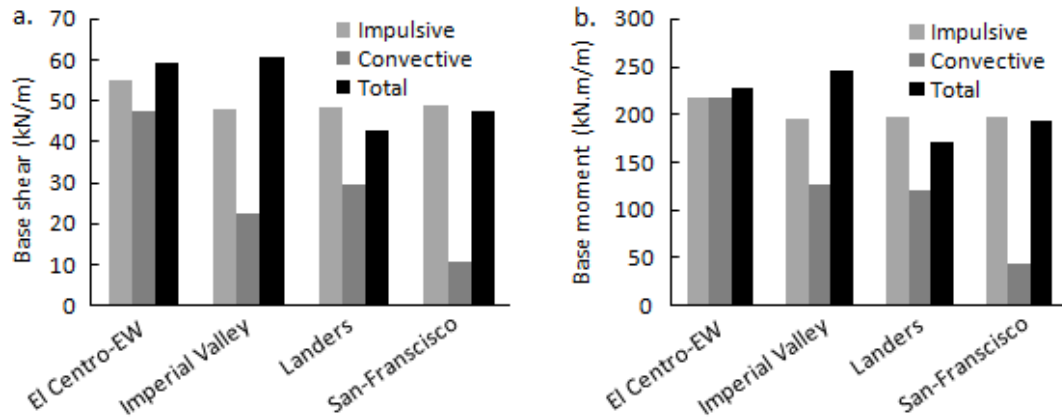


Fig. 14 Quantitative result of absolute maximum values of impulsive, convective and total hydrodynamic responses for different ground motions: (a) Base shear (b) Base moment

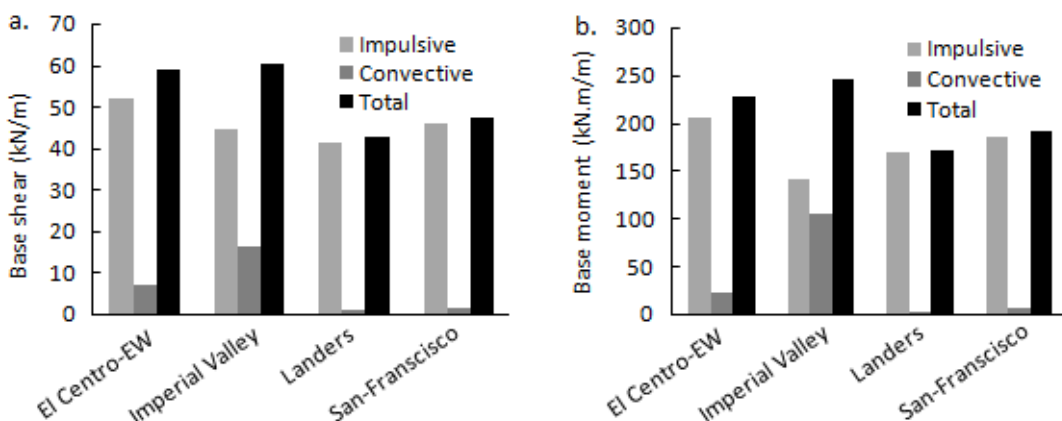


Fig. 15 Component-wise break up of peak hydrodynamic responses for different ground motions: (a) Base shear (b) Base moment

It is known that nonlinearity has no effect on the impulsive response since nonlinearity is associated with large amplitude sloshing and sloshing has nothing to do with impulsive response. Impulsive response being same in case of linear and nonlinear model the difference in overall dynamic behavior is decided by the difference in temporal variation of convective responses in case of linear and nonlinear model.

6.1.3 Pressure distribution on tank wall

The distributions of linear and nonlinear total hydrodynamic pressure on the container wall at the instant of maximum base shear are presented in Fig. 16. In case of low frequency ground motion of Imperial Valley, the nonlinear pressure resultant is more than the linear pressure resultant and the resultant height is also more than that of linear model. However, in case of intermediate and high frequency ground motions of Landers and San-Francisco respectively, the nonlinearity does not have major effect on the pressure distributions for the tank walls. The linear pressure resultants give conservative results for hydrodynamic force on the tank wall. However even though the pressure resultant in case of linear model is larger, the lower resultant height produces less overturning base moment than the nonlinear model and hence may give non-conservative result for overturning base moment. Hence nonlinearity of surface wave cannot be overruled by conservative result of hydrodynamic force on the wall even for high frequency motions.

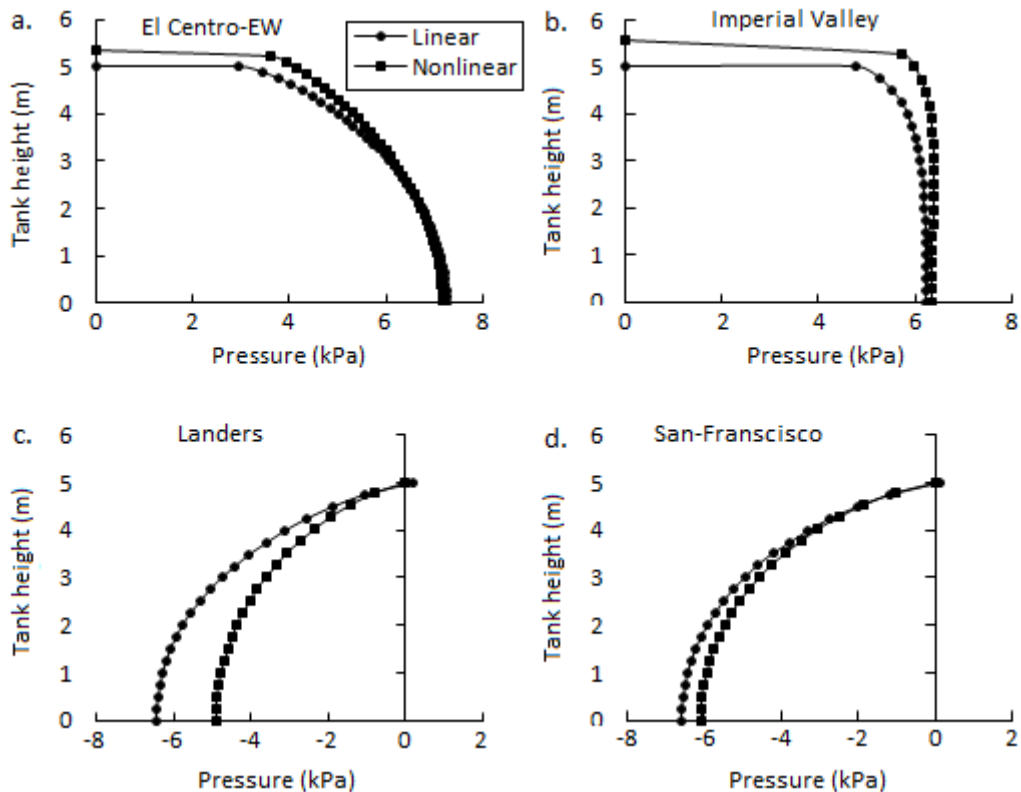


Fig. 16 Comparison of linear and nonlinear hydrodynamic pressure distribution along the height of tank wall: (a) El Centro-EW (b) Imperial Valley (c) Landers (d) San-Francisco

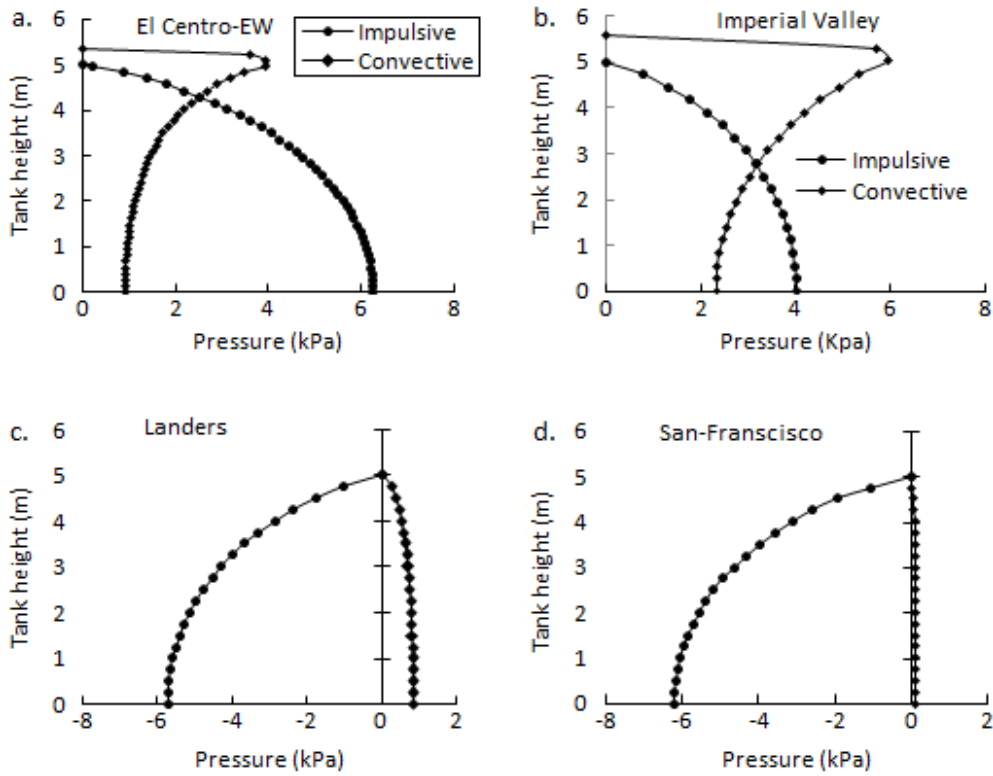


Fig. 17 Distribution of impulsive and convective nonlinear hydrodynamic pressure along the height of tank wall: (a) El Centro-EW (b) Imperial Valley (c) Landers (d) San-Francisco

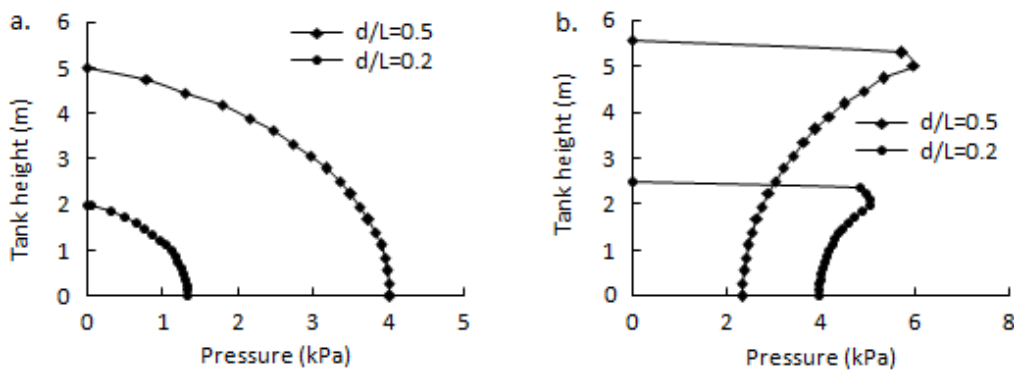


Fig. 18 Hydrodynamic pressure along the height of tank wall for Imperial Valley earthquake: (a) Impulsive (b) Convective

Fig. 17 shows the distributions of impulsive and convective responses of pressure at the instant of maximum base shear for all ground motions. One can observe considerably higher contribution of convective response due to Imperial Valley record as compared to other earthquakes. The convective pressure resultant acts high up the wall. This is consistent with the other responses presented in Table 4 and clarifies the confusion, if any, of the reader as mentioned in paragraph 3

of 6.1.2. The convective pressure resultant due to high frequency San-Francisco earthquake is negligibly small and that due to Landers is not appreciable compared to the impulsive response.

The indispensability of nonlinearity of surface wave is further buttressed in Fig. 18. The impulsive and convective pressure distributions due to tall and shallow tank are presented in Fig. 18. Significant increase in impulsive force is observed for tall tank of same width, which is due to the increased mass of liquid. The convective pressure at each point up to the depth of liquid in shallow tank is significantly more than those for the tall tank.

7. Conclusions

In the present study, an efficient Galerkin based two dimensional fully nonlinear finite element model has been developed for investigation and quantification of seismic behavior of partially filled rigid rectangular liquid tank under horizontal ground motions of different frequency content. Mixed Eulerian-Lagrangian (MEL) method based fourth order explicit Runge-Kutta scheme is used for the time-stepping integration of free surface boundary conditions. An artificial damping term μ is suitably introduced into the finite element formulation via modified surface boundary condition to mimic the surface damping on account of viscosity of liquid. It is defined as $\mu = 2\zeta\omega$ where ζ is the viscous type numerical damping and ω is the fundamental frequency of liquid and a value equal to 0.0075 is used for ζ . The model is capable of finding out both convective and impulsive responses of the hydrodynamic behavior. The effect of nonlinearity of surface wave on the convective response and hence on the overall hydrodynamic behaviour is investigated.

Four different horizontal ground motions with peak ground acceleration scaled to a constant value of 0.2g are applied to investigate the effect of frequency content of ground motion on the seismic behavior of tank-liquid system. Time history analysis of sloshing elevation, structural base shear, overturning base moment are carried out and the results of absolute maximum values of free surface wave elevation, structural base shear, overturning base moment are presented. In addition the absolute maximum responses of impulsive and convective components of hydrodynamic forces are presented. The hydrodynamic responses due to linear model are depicted for comparison. The hydrodynamic pressure distributions on tank wall at the instant of maximum base shear for the chosen ground motions are compared. For completeness of investigation, numerical experiment is also conducted in shallow tank to study the effect of tank geometry on the dynamic response and in so doing the only ground motion of low frequency Imperial Valley earthquake is selected as external excitation.

Important inferences drawn from the study may be summarized as follows:

1. In time domain analysis local temporal variation of nonlinear convective response and their contribution to total hydrodynamic forces is equally important if not more important than the absolute global peak of total dynamic response and ought to be considered for the design of tank because of cumulative structural damage sustained by the tank.
2. Nonlinearity of surface wave is not only important in shallow tank design but also critical in tall tanks subjected to low frequency ground motions and thus crucial in shaping the convective responses.
3. Contrary to the generally accepted notion of dominance of impulsive component on the hydrodynamic response, this study finds that although impulsive component dominates the hydrodynamic pressure in high frequency content earthquakes and also has a dominating share in total hydrodynamic response in all other ground motions, the convective components do also play

an important role in low frequency earthquakes.

4. Design should not be biased on the basis of conservativeness of linear total hydrodynamic pressure distribution on tank wall. This is because conservativeness of hydrodynamic pressure does not necessarily guarantee other responses to be also conservative.

References

- Bakhshi, A. and Hassanikhah, A. (2008), "Comparison between seismic responses of anchored and unanchored cylindrical steel tanks", *14th World Conference on Earthquake Engineering*, Beijing, China, October.
- Biswal, K.C., Bhattacharyya, S.K. and Sinha, P.K. (2006), "Non-linear sloshing in partially liquid filled containers with baffles", *Int. J. Numer. Meth. Eng.*, **68**, 317-337.
- Chen, B.F. and Chiang, H.W. (1999), "Complete 2D and fully nonlinear analysis of ideal fluid in tanks", *J. Eng. Mech.*, **125**(1), 70-78.
- Chen, W., Haroun, M.A. and Liu, F. (1996), "Large amplitude liquid sloshing in seismically excited tanks", *Earthq. Eng. Struct. Dyn.*, **25**, 653-669.
- Chen, Y.H., Hwang, W.S. and Ko, C.H. (2007), "Sloshing behaviours of rectangular and cylindrical liquid tanks subjected to harmonic and seismic excitations", *Earthq. Eng. Struct. Dyn.*, **36**, 1701-1717.
- Cho, J.R. and Lee, H.W. (2004), "Non-linear finite element analysis of large amplitude sloshing flow in two-dimensional tank", *Int. J. Numer. Meth. Eng.*, **61**, 514-531.
- Choun, Y.S. and Yun, C.B. (1999), "Sloshing analysis of rectangular tanks with a submerged structure by using small-amplitude water wave theory", *Earthq. Eng. Struct. Dyn.*, **28**, 763-783.
- Dommermuth, D.G. and Yue, D.K.P. (1987), "Numerical simulations of nonlinear axisymmetric flows with a free surface", *J. Fluid Mech.*, **178**, 195-219.
- Faltinsen, O.M. (1978), "A numerical nonlinear method of sloshing in tanks with two-dimensional flow", *J. Ship Research*, **22**(3), 193-202.
- Haroun, M.A. (1983), "Vibration studies and tests of liquid storage tank", *Earthq. Eng. Struct. Dyn.*, **11**, 190-206.
- Haroun, M.A. (1984), "Stress analysis of rectangular walls under seismically induced hydrodynamic loads", *Bull Seismol. Soc. Am.*, **74**(3), 1031-1041.
- Haroun, M.A. and Ellaithy, M.H. (1984), "Seismically induced fluid forced on elevated tanks", *J. Tech. Topic. Civ. Eng.*, **111**, 1-15.
- Haroun, M.A. and Tayel, M.A. (1985), "Response of tanks to vertical seismic excitations", *Earthq. Eng. Struct. Dyn.*, **13**, 583-95.
- Heidebrecht, A.C. and Lu, C.Y. (1988), "Evaluation of the seismic response factor introduced in the 1985 edition of the National Building Code of Canada", *Can. J. Civil Eng.*, **15**, 332-338.
- Hernandez-Barrrios, H., Heredia, E. and Alvaro, A. (2007), "Nonlinear sloshing response of cylindrical tanks subjected to earthquake ground motion", *Eng. Struct.*, **29**, 3364-3376.
- Housner, G.W. (1963), "The dynamic behavior of water tanks", *Bull Seismol. Soc. Am.*, **53**(2), 381-387.
- Lau, D.T., Marquez, D. and Qu, F. (1996), "Earthquake resistant design of liquid storage tanks", *11th World Conference on Earthquake Engineering*, Paper No. 1293.
- Leon, G.S. and Kausel, E.A.M. (1986), "Seismic analysis of fluid storage tanks", *J. Struct. Eng.*, **112**, 1-8.
- Longuet-Higgins, M.S. and Cokelet, E.D. (1976), "The deformation of steep surface wave on water: a numerical method of computation", *Proceedings of Royal Society of London*, **350**, 1-26.
- Malhotra, P.K. (1996), "Seismic uplifting of flexibly supported-storage tanks", *11th World conference of Earthquake Engineering*, Paper No. 873.
- Mitra, S. and Sihnamapatra, K.P. (2007), "Slosh dynamics of liquid-filled containers with submerged components using pressure-based finite element method", *J. Sound Vib.*, **304**, 361-381.
- Pal, N.C., Bhattacharyya, S.K. and Sinha, P.K. (2003), "Non-linear coupled slosh dynamics of liquid-filled

- laminated composite containers: a two dimensional finite element approach”, *J. Sound Vib.*, **261**, 729-749.
- Pal, P. and Bhattacharyya, S.K. (2010), “Sloshing in partially filled liquid containers-Numerical and experimental study for 2-D problems”, *J. Sound Vib.*, **329**, 4466-4485.
- Romero, V.J. and Ingber, M.S. (1995), “A numerical model for 2-D sloshing of pseudo-viscous liquids in horizontally accelerated rectangular containers”, *Boundary Element XVIII*, **1**, 567-583.
- Seleemah, A.A. and El-Sharkawy, M. (2011), “Seismic analysis and modelling of isolated elevated liquid storage tanks”, *Earthq. Struct.*, **2**(4), 397-412.
- Virella, J.C., Prato, C.A. and Godoy, L.A. (2008), “Linear and nonlinear 2D finite element analysis of sloshing modes and pressure in rectangular tanks subjected to horizontal harmonic motions”, *J. Sound Vib.*, **312**(3), 442-60.
- Wu, G.X. and Taylor, R.E. (1994), “Finite element analysis of two-dimensional non-linear transient water waves”, *Appl. Ocean Res.*, **16**, 363-372.